

ION DYNAMICS DURING THE PARAMETRIC INSTABILITIES OF A LEFT-HAND POLARIZED ALFVÉN WAVE IN A PROTON–ELECTRON–ALPHA PLASMA

XINLIANG GAO¹, QUANMING LU¹, XING LI², YUFEI HAO¹, XIN TAO¹, AND SHUI WANG¹

¹ CAS Key Laboratory of Geospace Environment, Department of Geophysics and Planetary Science,

University of Science and Technology of China, Hefei 230026, China; qmlu@ustc.edu.cn

² Institute of Mathematics and Physics, Aberystwyth University, Aberystwyth SY23 3BZ, UK

Received 2013 September 13; accepted 2013 November 7; published 2013 December 11

ABSTRACT

The parametric instabilities of an Alfvén wave in a proton–electron plasma system are found to have great influence on proton dynamics, where part of the protons can be accelerated through the Landau resonance with the excited ion acoustic waves, and a beam component along the background magnetic field is formed. In this paper, with a one-dimensional hybrid simulation model, we investigate the evolution of the parametric instabilities of a monochromatic left-hand polarized Alfvén wave in a proton–electron–alpha plasma with a low beta. When the drift velocity between the protons and alpha particles is sufficiently large, the wave numbers of the backward daughter Alfvén waves can be cascaded toward higher values due to the modulational instability during the nonlinear evolution of the parametric instabilities, and the alpha particles are resonantly heated in both the parallel and perpendicular direction by the backward waves. On the other hand, when the drift velocity of alpha particles is small, the alpha particles are heated in the linear growth stage of the parametric instabilities due to the Landau resonance with the excited ion acoustic waves. Therefore, the heating occurs only in the parallel direction, and there is no obvious heating in the perpendicular direction. The relevance of our results to the preferential heating of heavy ions observed in the solar wind within 0.3 AU is also discussed in this paper.

Key words: method: numerical – plasmas – solar wind – waves

Online-only material: color figures

1. INTRODUCTION

Alfvén waves are the exact solution of the ideal incompressible MHD equations regardless of their amplitude, and the intensity of their total magnetic field is constant. However, when the compression effect is taken into account, the Alfvén waves will become unstable to the parametric instabilities (Galeev & Oraevskii 1963; Goldstein 1978; Wong & Goldstein 1986; Jayanti & Hollweg 1993a, 1993b; Hollweg 1994; Gomberoff et al. 2001; Del Zanna et al. 2001; Nariyuki & Hada 2007), which has been a hot topic in the plasma community since the 1960s. Galeev & Oraevskii (1963) first studied the evolution of a monochromatic Alfvén wave and showed that it is unstable to the parametric decay in a low beta plasma. In the process of the decay instability, the energy of a pump Alfvén wave is gradually transferred to that of a forward ion acoustic wave and a backward daughter Alfvén wave. This instability might account for the radial decrease of normalized cross-helicity in the fast solar wind (Bavassano & Bruno 1989; Bruno et al. 1997, 2006). Another important parametric instability is the modulational instability, which involves a forward-propagating ion acoustic wave and two forward-propagating Alfvén waves (Derby 1978; Longtin & Sonnerup 1986; Nariyuki & Hada 2007; Nariyuki et al. 2007, 2009). The modulational instability is more likely to occur when the plasma beta is finite (Nariyuki & Hada 2007; Nariyuki et al. 2007) or the pump Alfvén waves have a spectrum (Nariyuki et al. 2007, 2008a).

Recently, the effects of the parametric instabilities on the evolution of the velocity distribution of particles began to attract attention (Araneda et al. 2008; Nariyuki et al. 2009; Matteini et al. 2010). Araneda et al. (2008) have shown that a proton beam can be formed during the modulational instability of an Alfvén wave, which is due to the Landau resonance with the excited ion acoustic waves. Matteini et al. (2010) investigated the parameter

instabilities in a large range of parameters. They found that such a deformation of the proton distribution function is a common consequence of the nonlinear particle trapping in the parametric instabilities, either the decay or modulational instability, where the ion acoustic waves are excited and then in resonance with the protons. These results may help us to understand the formation of the velocity distribution of the protons in the fast solar wind, which is usually composed of a tenuous beam component and an anisotropic core component (Feldman et al. 1973, 1974; Goodrich & Lazarus 1976; Marsch et al. 1982; Marsch 1991; Goldstein et al. 2000; Tu et al. 2004).

However, there always exist minor ions in the fast solar wind. Among these minor ions, alpha particles are the most common species with an abundance of about 4%, and they flow faster than the core protons with a drift velocity ranging from zero to about one local Alfvén speed (Marsch et al. 1982; von Steiger et al. 1995; von Steiger & Zurbuchen 2006; Bourouaine et al. 2013). With one-dimensional (1D) hybrid simulations, Araneda et al. (2009) have studied the evolution of the alpha particle distributions during the parametric instabilities of the Alfvén waves in a proton–electron–alpha plasma. They found that the alpha particles can be obviously heated in the parallel direction due to the resonant interaction with the ion acoustic waves, while the heating in the perpendicular direction is very weak. In their paper, there is no initial drift velocity between the protons and alpha particles.

In this work, with a 1D hybrid simulation model, we investigate ion dynamics during the parametric instabilities of a monochromatic parallel propagating Alfvén wave in a proton–electron–alpha plasma, and the effects of the drift velocity between the protons and alpha particles are considered. In our simulations, a low plasma beta ($\beta_p = 0.04$), which may be a typical value in the solar wind within 0.3 AU, is used. Such a small plasma beta of the solar wind is often produced in fast

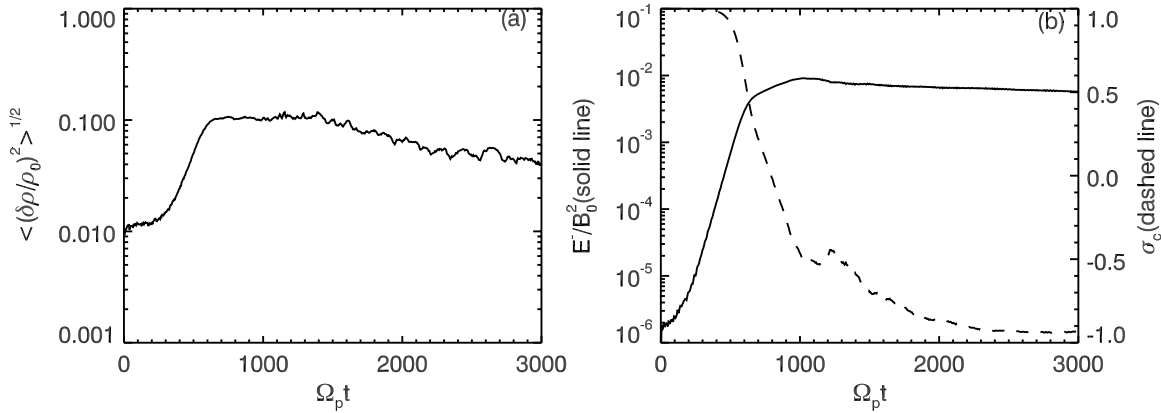


Figure 1. Time evolution of (a) the density fluctuations $\langle (\delta\rho/\rho_0)^2 \rangle^{1/2}$ and (b) the wave energy of backward-propagating Alfvén waves E^-/B_0^2 (solid line) and the normalized cross-helicity σ_c (dashed line) for Run 1.

solar wind models (Hu et al. 1997; Li et al. 1997, 1999) in the near Sun region. The results show that when the drift velocity is sufficiently large, the alpha particles can be heated in the perpendicular direction as well as in the parallel direction during a three-step process. First, a parametric decay is excited at the linear growth stage, and a backward daughter Alfvén wave is generated. Then, the frequency of the backward Alfvén wave is cascaded toward higher values during the nonlinear evolution of the parametric instabilities. Finally, the alpha particles are resonantly heated by the backward Alfvén waves.

The organization of this paper is as follows. The simulation model and plasma parameters are described in Section 2. The simulation results are illustrated in Section 3. Discussions and a summary are given in the last section.

2. SIMULATION MODEL

A 1D hybrid simulation model with periodic boundary conditions is used to investigate the ion dynamics during the parametric instabilities of a monochromatic left-hand polarized Alfvén wave in a proton–electron–alpha plasma with a low beta. Hybrid simulations treat ions as macroparticles, while electrons are assumed to be a massless fluid (Winske 1985; Quest 1988; Winske & Omid 1993). Therefore, electron dynamics are neglected, and the electron damping of the ion acoustic waves in the parametric instabilities is not considered. The simulations allow for one spatial direction, which is parallel to the background magnetic field ($B_0\hat{x}$).

We initialize the system with a monochromatic left-hand polarized Alfvén wave propagating along the background magnetic field, and the corresponding fluctuating magnetic field and transverse velocity are given by

$$\delta\mathbf{B}_w = \delta B [\cos(k_0x)\hat{y} + \sin(k_0x)\hat{z}] \quad (1)$$

$$\delta\mathbf{u}_i = \delta u_i [\cos(k_0x)\hat{y} + \sin(k_0x)\hat{z}] \quad (2)$$

and they satisfy the Walen’s relation (Nariyuki et al. 2009; Matteini et al. 2010):

$$\delta\mathbf{u}_i = \frac{e_i}{m_i} \frac{\omega_0/k_0 - U_{i0}}{\omega_0 - U_{i0}k_0 - \Omega_i} \delta\mathbf{B}_w \quad (3)$$

where i represents the ion species, U_{i0} is the bulk velocity along the background magnetic field, and Ω_i is the gyrofrequency. In our simulations, two ion species are considered: protons and

Table 1
Summary of Simulations (Runs 1–4)

Run	k_0c/ω_{pp}	ω_0/Ω_p	$U_{\alpha p}/V_A$
1	0.209	0.176	1.0
2	0.209	0.176	0.0
3	0.209	0.179	0.8
4	0.209	0.181	0.5

Note. where V_A is the Alfvén speed.

alpha particles, which are represented with p and α , respectively. ω_0 and k_0 are the frequency and wave number of the pump wave. The amplitude of the pump wave $\delta B/B_0$ is set to be 0.2, and its dispersion relation is derived from the MHD equations in a cold proton–electron–alpha plasma (Baumjohann & Treumann 1997):

$$-n_p e_p \frac{(\omega_0 - U_{p0}k_0)^2}{\omega_0 - U_{p0}k_0 - \Omega_p} - n_\alpha e_\alpha \frac{(\omega_0 - U_{\alpha0}k_0)^2}{\omega_0 - U_{\alpha0}k_0 - \Omega_\alpha} = k_0^2 \quad (4)$$

where n_i is the number density.

Initially, all ion species satisfy the Maxwellian velocity distribution, and the temperature of the alpha particles is the same as that of the protons. The proton beta β_p is 0.04, while the electron beta β_e is 0.1. We choose the number density of the alpha particles as $n_\alpha/n_e = 4\%$ (where $n_e = n_p + 2n_\alpha$ is the number density of the electrons). In total, four runs are performed. The wave number k_0 and frequency ω_0 of the pump wave and the relative drift velocity between the alpha particles and protons $U_{\alpha p}$ for the four runs are illustrated in Table 1.

The number of grid cells is $n_x = 600$, and the size of the grid cell is $\Delta x = 1.0c/\omega_{pp}$ (where c/ω_{pp} is the proton inertial length, c is the light speed, and ω_{pp} is the proton plasma frequency based on total number density n_e). There are on average ~ 900 macroparticles in every cell for each ion species. The simulations are performed in the center-of-mass frame, where the charge neutrality ($\sum_i e_i n_i = 0$, where i denotes the species of particles) and the zero current condition ($\sum_i e_i n_i U_{i0} = 0$) are satisfied initially. The time step is $\Omega_p \Delta t = 0.025$.

3. SIMULATION RESULTS

In Figure 1, we first exhibit the time evolution of (1) the density fluctuation $\langle (\delta\rho/\rho_0)^2 \rangle^{1/2}$ (where ρ_0 is the initial density), (2) the normalized cross-helicity $\sigma_c = (E^+ - E^-)/(E^+ + E^-)$ (where

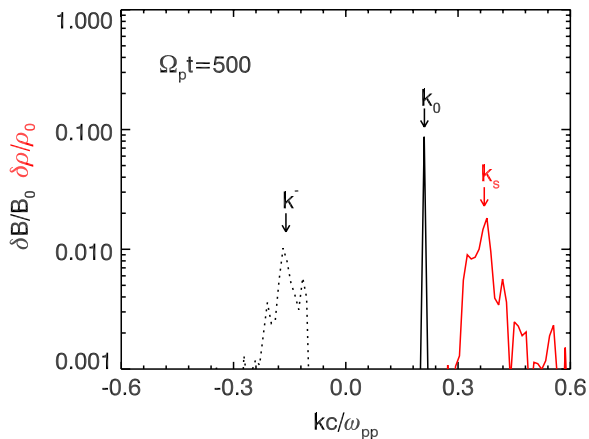


Figure 2. Power spectra for the fluctuations of the magnetic field and density at $\Omega_p t = 500$ for Run 1. The black lines and red lines represent the magnetic and density fluctuations, respectively. The forward modes and backward modes are denoted by the solid lines and dashed lines, respectively. The pump wave, primary ion acoustic wave, and daughter Alfvén wave are marked by arrows. (A color version of this figure is available in the online journal.)

E^+ and E^- denote the energy of the Alfvén waves propagating forward and backward, respectively) and E^-/B_0^2 for Run 1. Here, the cross-helicity σ_c measures the Alfvénicity of the magnetic fluctuations in the system. We can obtain the magnetic fluctuations of the forward and backward Alfvén waves by separating the magnetic fluctuations into positive and negative helical parts with the method developed by Terasawa et al. (1986). For a left-hand polarized pump Alfvén wave, the negative helical part corresponds to forward-propagating waves, whereas the positive helical part corresponds to backward-propagating waves. The instability is excited at about $\Omega_p t = 350$, and both the density fluctuation and the energy of the backward daughter waves begin to increase rapidly at that time. At about $\Omega_p t = 800$, the instability gradually approaches the saturation stage, with the density fluctuation $\langle(\delta\rho/\rho_0)^2\rangle^{1/2} \approx 0.15$ and the energy of the backward daughter waves $E^-/B_0^2 \approx 0.01$. This process is quite similar to the parametric decay of a parallel propagating Alfvén wave in a proton–electron plasma

(Del Zanna et al. 2001; Matteini et al. 2010; Gao et al. 2013a). In addition, during the linear growth phase of the decay instability, the cross-helicity σ_c shows a sharp decrease, from 1.0 to ~ -0.3 . Then, the cross-helicity decreases slowly till the end of our simulation, with $\sigma_c \approx -0.9$, and at that time the amplitude of the backward daughter waves is much larger than that of the forward-propagating waves.

Figure 2 shows the power spectra of the magnetic fluctuations and density at $\Omega_p t = 500$ for Run 1. At $\Omega_p t = 500$, the parametric decay has already been excited. Besides the pump Alfvén wave with the wave number $k_0 c/\omega_{pp} \approx 0.21$, we can also identify two other wave modes: the ion acoustic waves and the backward daughter Alfvén waves. The wave number of the ion acoustic waves with the largest amplitude is at $k_s c/\omega_{pp} \approx 0.39$, while the wave number of the daughter Alfvén waves with the largest amplitude is $k^- c/\omega_{pp} \approx -0.18$. They satisfy the three-wave resonant condition $k^- = k_0 - k_s$.

To investigate the effects of the parametric instabilities on the proton velocity distribution function, in Figure 3 we plot the scatter plots of the protons in the $(v_{||p}, v_{\perp p})$ space for Run 1 at $\Omega_p t = 0$ and 800. In the figure, the particles in one fixed cell are recorded. At $\Omega_p t = 0$, the protons satisfy the Maxwellian distribution, which is marked by the red dashed line in Figure 3(a). Besides, these particles have a bulk velocity about $0.2V_A$ in the perpendicular direction due to their coupling with the magnetic fluctuations. At the saturation stage of the instability (shown at $\Omega_p t = 800$), a beam-like component is formed along the background magnetic field, which is generated by the Landau resonance with the excited ion acoustic waves. Such a process has already been investigated in previous works (Araneda et al. 2008; Araneda et al. 2009; Matteini et al. 2010). If we separate the protons into the core and beam components, although there is no obvious heating of the core protons (denoted by a red dashed line in Figure 3(b)), they also exhibit an obvious temperature anisotropy due to the formation of the beam component.

We also study the impact of parametric instabilities on the behaviors of the alpha particles. Figure 4 displays the time evolution of the parallel temperature $T_{||\alpha}/T_{0\alpha}$ and the perpendicular temperature $T_{\perp\alpha}/T_{0\alpha}$ (where $T_{0\alpha}$ is the initial

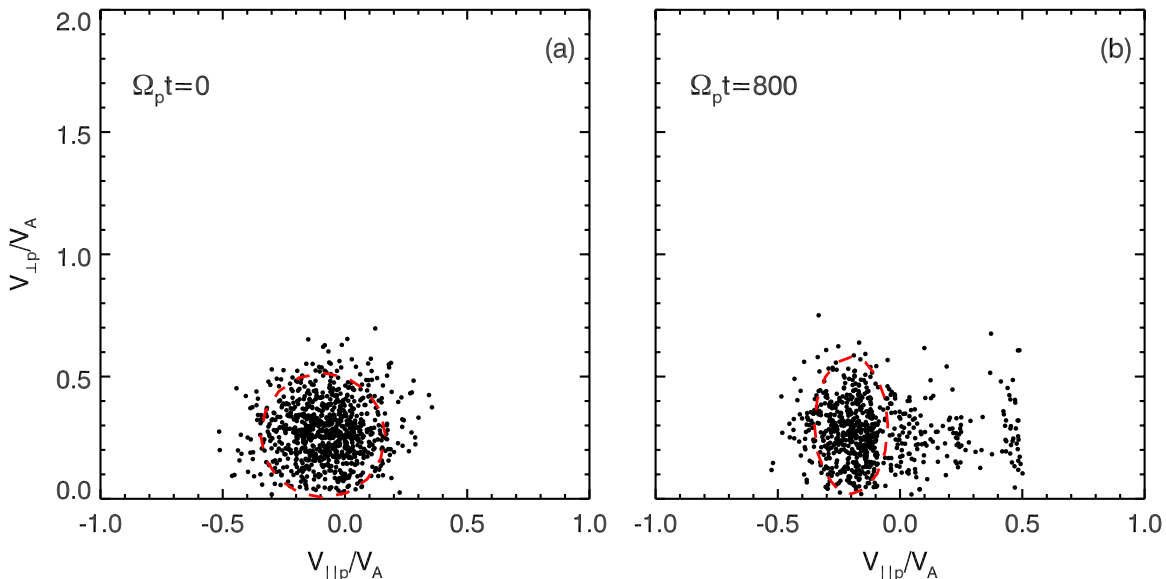


Figure 3. Scatter plots of protons in the $(v_{||p}, v_{\perp p})$ space for Run 1. The core components are marked by red dashed lines. (A color version of this figure is available in the online journal.)

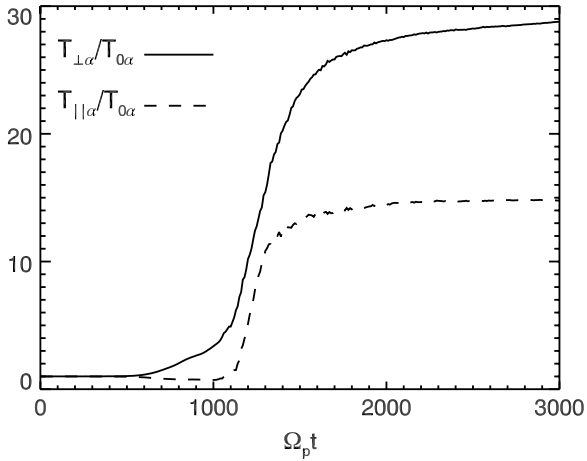


Figure 4. Time evolution of the parallel temperature $T_{\parallel\alpha}/T_{0\alpha}$ (dashed line) and the perpendicular temperature $T_{\perp\alpha}/T_{0\alpha}$ (solid line) of alpha particles for Run 1.

temperature of the alpha particles) for Run 1. At first, we calculate the parallel temperature of the alpha particles with $T_{\parallel\alpha} = m_{\alpha}\langle(v_x - \langle v_x \rangle)^2\rangle$ and the perpendicular temperature with $T_{\perp\alpha} = m_{\alpha}\langle(v_y - \langle v_y \rangle)^2 + (v_z - \langle v_z \rangle)^2\rangle/2$ in every grid cell (where the bracket $\langle \bullet \rangle$ denotes an average over one grid cell), and then the temperatures are obtained by averaging them over all grids. With this method, the effects of the bulk velocity at each location on the calculated temperatures can be eliminated (Lu et al. 2009; Lu & Chen 2009; Gao et al. 2012, 2013b). From Figure 4, it is found that the alpha particles can be obviously heated, and the heating is preferentially in the perpendicular direction. At the end of simulation, the perpendicular and parallel temperatures increase to about 29 and 15 times their corresponding initial values. Moreover, it is worth noting that the heating of the alpha particles only occurs after the saturation of the parametric decay rather than in the linear growth phase.

In order to reveal what mechanisms are playing a critical role in the heating of the alpha particles, in Figure 5 we plot the

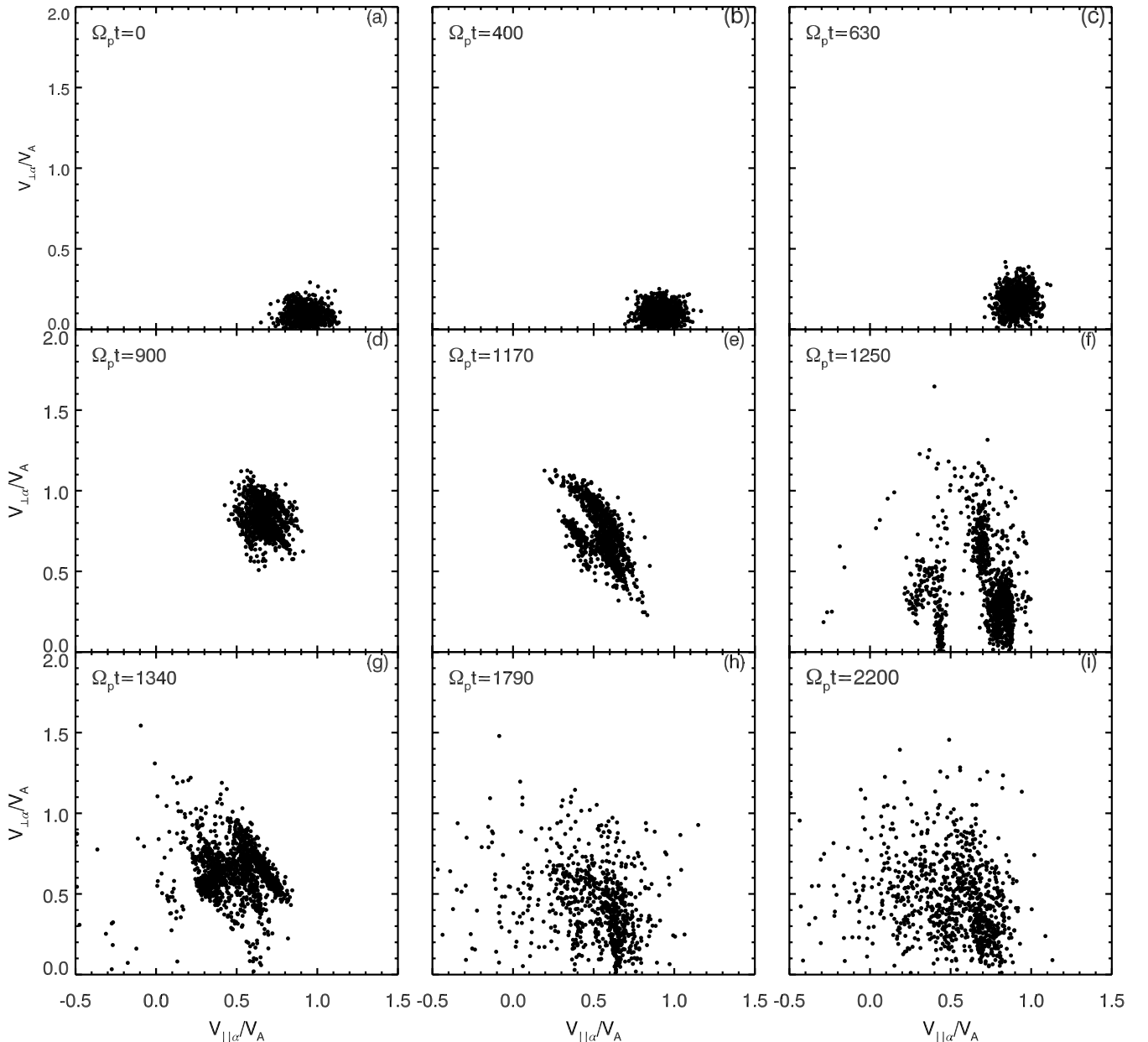


Figure 5. Scatter plots of alpha particles in the $(v_{\parallel\alpha}, v_{\perp\alpha})$ space for Run 1.

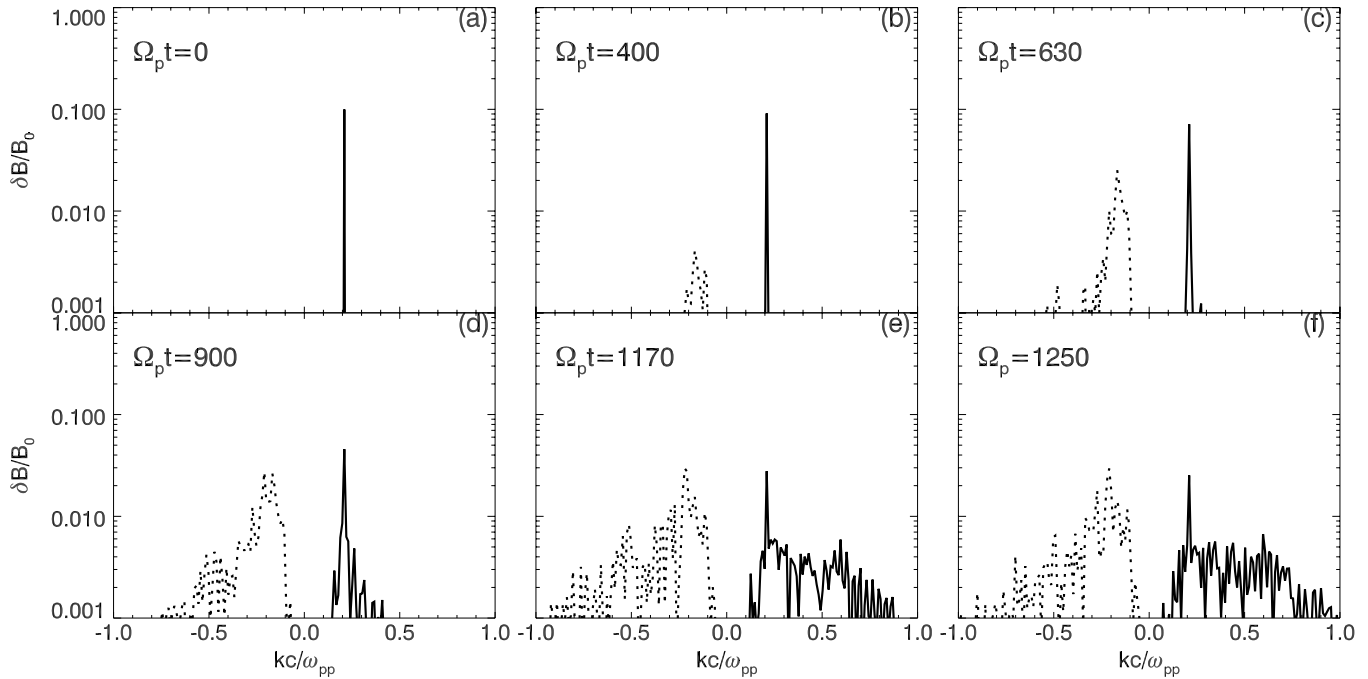


Figure 6. Power spectra for the fluctuations of the magnetic field for Run 1. The forward modes and backward modes are denoted by the solid lines and dashed lines, respectively.

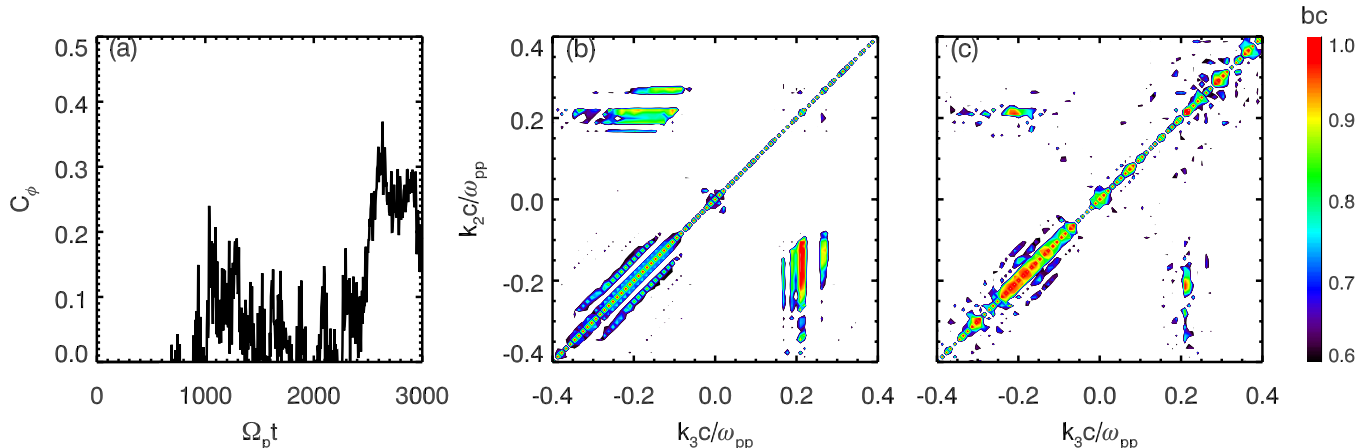


Figure 7. (a) Time evolution of phase coherence index for Run 1. The bicoherence index $bc(k_1, k_2, k_3)$ for the periods (b) $400-600 \Omega_p^{-1}$ and (c) $1000-1200 \Omega_p^{-1}$ for Run 1.

(A color version of this figure is available in the online journal.)

evolution of the velocity distribution of the alpha particles in the $(v_{\parallel\alpha}, v_{\perp\alpha})$ space for Run 1, while the evolution of power spectra for the fluctuations of the magnetic field is shown in Figure 6. During the linear growth stage of the parametric decay, there is no obvious heating for the alpha particles because they are not in resonance with the backward daughter waves. This is also consistent with the results in Figure 4. From about $\Omega_p t = 900$, the wave numbers of the backward Alfvén waves begin to cascade toward larger values, and then they can resonantly interact with the alpha particles, which results in the heating of the alpha particles. However, at first the distribution of the alpha particles is not so smooth, because we assume that the pump wave is monochromatic. As the spectrum of the backward waves extends to even larger wave numbers, the motion of alpha particles becomes more and more irregular due to the dispersion of these waves (Lu & Wang 2006). Finally, such motions result

in the formation of a nearly bi-Maxwellian distribution with a smaller drift velocity of $\sim 0.5 V_A$.

In Figure 7, we illustrate (a) the time evolution of the phase coherence index C_ϕ , the bicoherence index $bc(k_1, k_2, k_3) = |\langle \rho_{k_1} b_{k_2} b_{k_3}^* \rangle| / \sqrt{\langle |\rho_{k_1} b_{k_2}|^2 \rangle \langle |b_{k_3}^*|^2 \rangle}$ (where $k_3 = k_1 + k_2$ and the bracket $\langle \bullet \rangle$ denotes an average over a time interval) for the periods (b) $400-600 \Omega_p^{-1}$ and (c) $1000-1200 \Omega_p^{-1}$ for Run 1. The phase coherence C_ϕ for the waves with $k < 0$ is calculated with the same procedure developed by Nariyuki et al. (2009). The generation of phase coherence is a typical characteristic of the modulational instability (Nariyuki & Hada 2006), which is indicated by a finite value of C_ϕ (Nariyuki et al. 2009). From Figure 7(a), we can find that the modulational instability of the daughter Alfvén waves becomes important during the nonlinear evolution of the parametric instabilities (after about $\Omega_p t = 800$), and the wave numbers of the backward Alfvén waves begin to

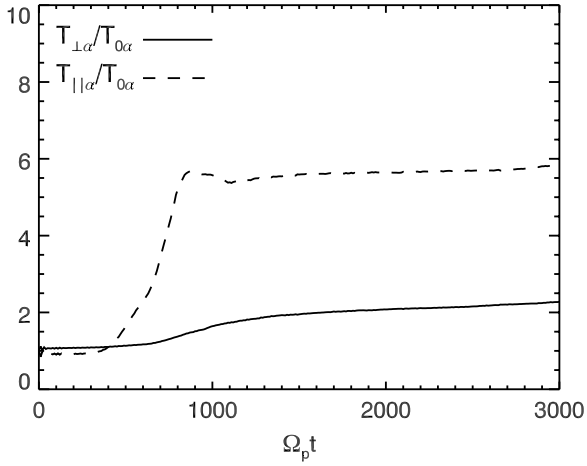


Figure 8. Time evolution of the parallel temperature $T_{||\alpha}/T_{0\alpha}$ (dashed line) and the perpendicular temperature $T_{\perp\alpha}/T_{0\alpha}$ (solid line) of alpha particles for Run 2.

cascade toward larger values as shown in Figure 6(d). This conclusion can also be confirmed by the bicoherence index in Figures 7(b) and (c). When $bc \sim 1$, it means that the wave number modes are in strong resonance (Diamond et al. 2000; Nariyuki & Hada 2006; Nariyuki et al. 2009). The strong resonance is observed in the region with $k_2 k_3 < 0$ in Figure 7(b), which is consistent with the parametric decay of the pump wave. However, in Figure 7(c), the waves with $k_2 k_3 > 0$ are in strong

resonance, showing that the modulational instability becomes important after the saturation of the decay instability. Therefore, we can conclude that the wave numbers of the backward Alfvén waves are cascaded toward larger values due to the modulational instability, and then they resonantly heat the alpha particles.

We also consider the effects of the drift velocity on the heating process of the alpha particles. Figure 8 displays the time evolution of the parallel temperature $T_{||\alpha}/T_{0\alpha}$ and the perpendicular temperature $T_{\perp\alpha}/T_{0\alpha}$ for Run 2. In this case, there is no relative drift velocity between the two ion species. There is no obvious heating of the alpha particles in the perpendicular direction. The parallel heating of the alpha particles that occurs in the linear growth stage of the parametric decay is mainly due to the Landau resonance with the excited ion acoustic waves. These results are consistent with that in Aranea et al. (2009). Compared with Run 1, the parallel heating of the alpha particles in Run 2 also becomes weaker than that in Run 1, with only ~ 6 times the initial temperature at the end of the simulation.

Figure 9 shows the velocity distribution of the alpha particles in the $(v_{||\alpha}, v_{\perp\alpha})$ space and the corresponding power spectra for the magnetic fluctuations at $\Omega_p t = 450, 800,$ and 2500 for Run 2. During the linear growth phase of the parametric decay (from about $\Omega_p t = 450$ to 800), the alpha particles can be heated in the parallel direction, which is mainly due to the Landau resonance with the excited ion acoustic waves. Then, the velocity distribution of the alpha particles stays almost unchanged, and no further heating can be obviously found. During the whole process of the parametric instabilities,

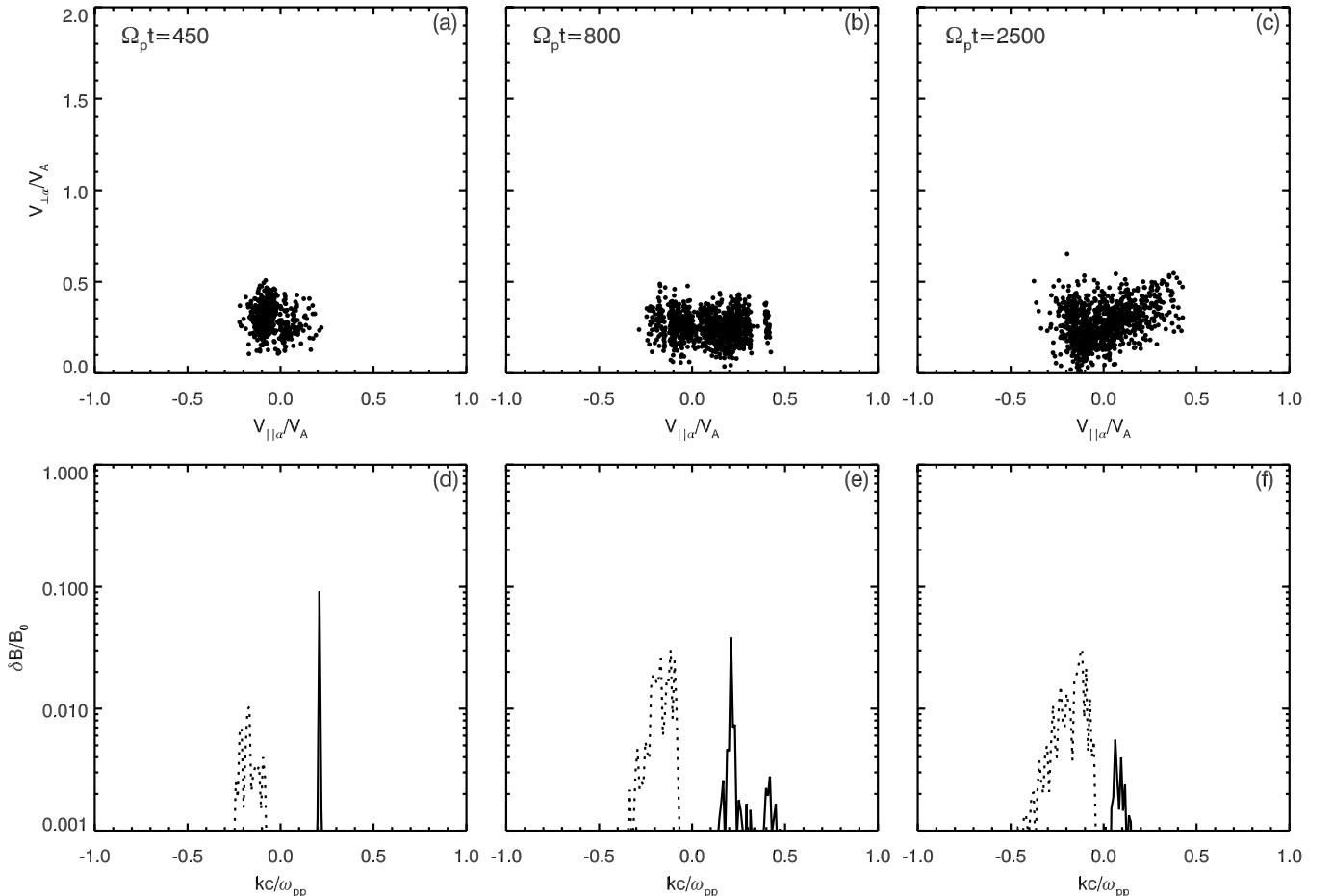


Figure 9. Scatter plots of alpha particles in the $(v_{||\alpha}, v_{\perp\alpha})$ space and the corresponding power spectra for the magnetic fluctuations at $\Omega_p t = 450, 800,$ and 2500 for Run 2. The forward modes and backward modes are denoted by the solid lines and dashed lines, respectively.

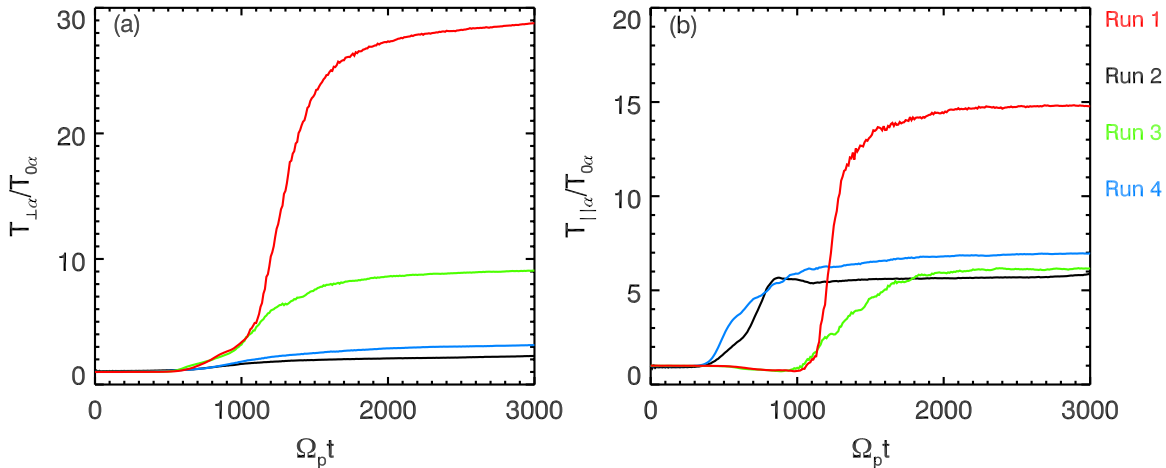


Figure 10. Time evolution of (a) the perpendicular temperatures of the alpha particles $T_{\perp\alpha}/T_{0\alpha}$ and (b) the parallel temperatures of the alpha particles $T_{\parallel\alpha}/T_{0\alpha}$ for Runs 1–4. The results for Runs 1–4 are denoted by the red, black, green, and blue lines, respectively.

(A color version of this figure is available in the online journal.)

there is almost no obvious perpendicular heating for the alpha particles. This is probably due to the small drift velocity of the alpha particles, which makes the cyclotron resonance condition between the backward Alfvén waves and the alpha particles hard to satisfy.

In Figure 10, the time evolution of (1) the perpendicular temperatures of the alpha particles $T_{\perp\alpha}/T_{0\alpha}$ and (2) the parallel temperatures of the alpha particles $T_{\parallel\alpha}/T_{0\alpha}$ for Runs 1–4 is displayed. For all runs, the parametric decay occurs and saturates at nearly the same time (not shown here). From Figure 10(a), we can find that the perpendicular heating occurs only after the saturation stage of the parametric decay, where the frequency of the backward Alfvén waves is cascaded toward higher values due to the modulational instability. Meanwhile, with the decrease of the drift velocity of the alpha particles, the perpendicular heating becomes weaker, and it is almost negligible in Runs 2 and 4. The reason is that the alpha particles with small drift velocity cannot resonantly interact with the backward Alfvén waves. Although the alpha particles can be heated in the parallel direction in all runs, there are still some differences. For Runs 1 and 3, the heating is caused by the resonant interactions of the alpha particles with the backward Alfvén waves, and it occurs after the saturation of the parametric decay. For Runs 2 and 4, the heating occurs during the linear growth phase of the parametric decay, which is mainly due to the Landau resonance with the excited ion acoustic waves.

4. CONCLUSIONS AND DISCUSSION

In this paper, with a 1D hybrid simulation model we have studied ion dynamics during the parametric instabilities of a monochromatic Alfvén wave in a proton–electron–alpha beam plasma with a low beta. At the linear growth stage, the pump Alfvén wave is unstable to the parametric decay, and the forward ion acoustic waves and backward daughter Alfvén waves are generated. Through the Landau resonance, part of the protons can be accelerated by these ion acoustic waves and form a beam component along the background magnetic field. The formed proton beam has also been found in previous studies of the parametric instabilities of an Alfvén wave (Araneda et al. 2008, 2009; Nariyuki et al. 2009; Matteini et al. 2010), which is considered to be relevant to the observed proton velocity distributions in the fast solar wind (Feldman et al. 1973, 1974;

Goodrich & Lazarus 1976; Marsch et al. 1982; Marsch 1991; Goldstein et al. 2000; Tu et al. 2004).

However, we further find that when the drift velocity between the protons and alpha particles is sufficiently large, the frequency of the backward daughter Alfvén waves can be cascaded toward higher values due to the modulational instability during the nonlinear evolution of the parametric instabilities, and the alpha particles are then heated due to the resonant interactions with the backward Alfvén waves. The heating can occur in both the parallel and perpendicular directions, which results in the temperature anisotropy of the alpha particles. When the drift velocity of the alpha particles is small, the resonance condition between the backward Alfvén waves and alpha particles cannot be satisfied, and the alpha particles are only heated during the linear growth stage due to the Landau resonance with the excited ion acoustic waves. The heating occurs only in the parallel direction, and there is no obvious heating in the perpendicular direction.

In situ measurements of the fast solar wind and remote sensing observations of the solar corona have revealed that the heavy minor ions are faster and hotter than the protons, and they generally are preferentially heated in the perpendicular direction (Feldman et al. 1974; Marsch et al. 1982; Kohl et al. 1998; Li et al. 1998; von Steiger & Zurbuchen 2006; Marsch 2006). Although the physical mechanisms responsible for the observed ion behavior are still in debate, it is commonly believed that the dissipation of Alfvén waves may be relevant to the observed ion heating. Our simulations have shown that in a low beta plasma ($\beta_p = 0.04$ is used in our simulations), when the alpha particles have a sufficiently large drift velocity, they can be resonantly heated by the generated backward-propagating Alfvén waves in both the parallel and perpendicular directions during the nonlinear evolution of the parametric instabilities of an Alfvén wave. The plasma beta is usually smaller than 0.1 in models of the fast solar wind within 0.3 AU (for instance, Hu et al. 1997; Li et al. 1997, 1999), and our results may provide a possible explanation for the heating of the minor ions observed in these regions. The importance of the backward-propagating Alfvén waves to continuous heating and formation of the high thermal anisotropy of O^{5+} observed at about 3–3.5 solar radii by the Ultraviolet Coronagraph Spectrometer on the *Solar and Heliospheric Observatory* in the solar corona has been emphasized by Hollweg (2006) since forward parallel

propagating ion cyclotron waves can rapidly lose resonance with minor ions when they have a drift flow speed faster than protons at >0.2 Alfvén speed. Within about 4 solar radii, the flow speed of oxygen ions is already substantially higher than the flow speed of protons (Kohl et al. 1998; Li et al. 1998). The proposed mechanism may play a role in the heating of minor ions at that distance and beyond.

Several limitations of our simulations should be discussed. The first point is that we use a monochromatic Alfvén wave as a pump wave. However, the Alfvénic fluctuations in the solar wind always have a broad spectrum, and the wave power at each primary mode is small. Therefore, the growth rate of the parametric instabilities may be significantly reduced and will need further study. The excited daughter waves should also have a broad spectrum. Second, the heating of alpha particles proposed in this paper relies on the produced backward-propagating Alfvén waves having sufficiently large wave numbers to make cyclotron resonant interaction between these waves and the alpha particles possible. This also requires that the wave number of the pump Alfvén wave must be sufficiently large. However, in situ measurements often find that low frequency waves in the solar wind usually carry much more power than their high frequency counterparts. It is an open question that whether Alfvén waves at frequencies not much smaller than ion gyrofrequencies can have sufficient power within 0.3 AU, although such ideas have been proposed (Axford & McKenzie 1992; Tu & Marsch 1997).

Third, this study only investigates the effect of a parallel propagating pump Alfvén wave. Multispacecraft measurement of solar wind magnetic field fluctuations at the ion gyro-radius or inertial scales often show that the dominant power of fluctuations is in directions of almost perpendicular (to the background magnetic field) propagation (Sahraoui et al. 2010; Narita et al. 2011; Roberts et al. 2013). A less powerful parallel propagating component may also exist (He et al. 2011; Podesta and Gary 2011). The data used for these studies are obtained at 1 AU or beyond, not in regions that the results of this paper can directly apply to (3 solar radii to 0.3 AU). However, one could speculate that in situ measured magnetic field fluctuations may be representative of those in the near-Sun region. It is recognized that very obliquely propagating pump waves may have stronger nonlinear effects than parallel propagating waves. Hence, the limitation of studying the decay of a parallel propagating pump wave may not be serious for understanding the nonlinear decay of pump waves.

Finally, all hybrid simulation models neglect electron dynamics. However, electron dynamics may have great influence on the parametric instabilities, which may damp the ion acoustic waves and then suppress the parametric instabilities. With a particle-in-cell simulation model, which includes electron dynamics, Nariyuki et al. (2008b) found that the electrons can be heated during the parametric instabilities of a large-amplitude, monochromatic Alfvén wave. How this point will influence the evolution of the parametric instabilities and the particle dynamics is for our future investigations.

This research was supported by the National Science Foundation of China, Grant Nos. 41174124, 41274144, 41331067, 41121003, the 973 Program (2012CB825602, 2013CBA01503), CAS Key Research Program KZZD-EW-01, and Ministry of Education (Grant No. IRT1190).

REFERENCES

- Araneda, J. A., Maneva, Y., & Marsch, E. 2009, *PhRvL*, **102**, 175001
 Araneda, J. A., Marsch, E., & Vinas, A. F. 2008, *PhRvL*, **100**, 125003
 Axford, W. I., & McKenzie, J. F. 1992, in Proc. 3rd COSPAR Colloquium, The Origin of High Speed Solar Wind Streams, in Solar Wind Seven, Goslar, Germany, 1991 September 16–20 (A93–33554 13–92), **1**
 Bavassano, B., & Bruno, R. 1989, *JGR*, **94**, 11977
 Baumjohann, W., & Treumann, R. A. 1997, *Basic Space Plasma Physics* (London: Imperial College Press)
 Bourouaine, S., Verscharen, D., Chandran, B. D. G., Maruca, B. A., & Kasper, J. C. 2013, *ApJL*, **777**, L3
 Bruno, R., Bavassano, B., D'Amicis, R., et al. 2006, *SSRv*, **122**, 321
 Bruno, R., Bavassano, B., Pietropaolo, E., Carbone, V., & Rosenbauer, H. 1997, *JGR*, **102**, 14687
 Del Zanna, L., Velli, M., & Londrillo, P. 2001, *A&A*, **367**, 705
 Derby, N. F. 1978, *ApJ*, **224**, 1013
 Diamond, P. H., Rosenbluth, M. N., Sanchez, E., et al. 2000, *PhRvL*, **84**, 4842
 Feldman, W. C., Asbridge, J. R., Bame, S. J., & Montgomery, M. D. 1973, *JGR*, **78**, 2017
 Feldman, W. C., Asbridge, J. R., Bame, S. J., & Montgomery, M. D. 1974, *RvGeo*, **12**, 715
 Galeev, A. A., & Oraevskii, V. N. 1963, *SPhD*, **7**, 988
 Gao, X. L., Lu, Q. M., Li, X., Huang, C., & Wang, S. 2012, *PhPI*, **19**, 032901
 Gao, X. L., Lu, Q. M., Li, X., Shan, L. C., & Wang, S. 2013a, *PhPI*, **20**, 072902
 Gao, X. L., Lu, Q. M., Li, X., Shan, L. C., & Wang, S. 2013b, *ApJ*, **764**, 71
 Goldstein, B. E., Neugebauer, M., Zhang, L. D., & Gary, S. P. 2000, *GeoRL*, **27**, 53
 Goldstein, M. L. 1978, *ApJ*, **219**, 700
 Gomberoff, L., Gomberoff, K., & Brinca, A. L. 2001, *JGR*, **106**, 18713
 Goodrich, C. C., & Lazarus, A. J. 1976, *JGR*, **81**, 2750
 He, J., Marsch, E., Tu, C., Yao, S., & Tian, H. 2011, *ApJ*, **731**, 85
 Hollweg, J. V. 1994, *JGR*, **99**, 23431
 Hollweg, J. V. 2006, *JGR*, **111**, A12106
 Hu, Y.-Q., Esser, R., & Habbal, S. R. 1997, *JGR*, **102**, 14661
 Jayanti, V., & Hollweg, J. V. 1993a, *JGR*, **98**, 19049
 Jayanti, V., & Hollweg, J. V. 1993b, *JGR*, **98**, 13247
 Kohl, J. L., Noci, G., Antonucci, E., et al. 1998, *ApJL*, **501**, L127
 Li, X., Esser, R., & Habbal, S. R. 1997, *JGR*, **102**, 17419
 Li, X., Habbal, S. R., Hollweg, J. V., & Esser, R. 1999, *JGR*, **104**, 2521
 Li, X., Habbal, S. R., Kohl, J. L., & Noci, G. 1998, *ApJL*, **501**, L133
 Longtin, M., & Sonnerup, B. U. O. 1986, *JGR*, **91**, 6816
 Lu, Q. M., & Chen, L. 2009, *ApJ*, **704**, 743
 Lu, Q. M., Du, A., & Li, X. 2009, *PhPI*, **16**, 042901
 Lu, Q. M., & Wang, S. 2006, *JGR*, **111**, A05204
 Marsch, E. 1991, in *Physics of the Inner Heliosphere, Vol. 2, Particles, Waves and Turbulence*, ed. R. Schween & E. Marsch (New York: Springer), **45**
 Marsch, E. 2006, *LRSP*, **3**, 1
 Marsch, E., Muhlhauser, K. H., Schwenn, R., et al. 1982, *JGR*, **87**, 52
 Matteini, L., Landi, S., Velli, M., & Hellinger, P. 2010, *JGR*, **115**, A09106
 Narita, Y., Gary, S. P., Saito, S., Glassmeier, K. H., & Motschmann, U. 2011, *GeoRL*, **38**, 5
 Nariyuki, Y., & Hada, T. 2006, *NPGeo*, **13**, 425
 Nariyuki, Y., & Hada, T. 2007, *JGR*, **112**, A10107
 Nariyuki, Y., Hada, T., & Tsubouchi, K. 2007, *PhPI*, **14**, 122110
 Nariyuki, Y., Hada, T., & Tsubouchi, K. 2008a, *PhPI*, **15**, 114502
 Nariyuki, Y., Hada, T., & Tsubouchi, K. 2009, *JGR*, **114**, A07102
 Nariyuki, Y., Matsukiyo, S., & Hada, T. 2008b, *NJPh*, **10**, 083004
 Podesta, J. J., & Gary, S. P. 2011, *ApJ*, **734**, 15
 Quest, Q. B. 1988, *JGR*, **93**, 9649
 Roberts, O. W., Li, X., & Li, B. 2013, *ApJ*, **769**, 58
 Sahraoui, F., Goldstein, M. L., Belmont, G., Canu, P., & Rezeau, L. 2010, *PhRvL*, **105**, 131101
 Terasawa, T., Hoshino, M., Sakai, J.-I., & Hada, T. 1986, *JGR*, **91**, 4171
 Tu, C.-Y., & Marsch, E. 1997, *SoPh*, **171**, 363
 Tu, C.-Y., Marsch, E., & Qin, Z.-R. 2004, *JGR*, **109**, A05101
 von Steiger, R., Geiss, J., Gloeckler, G., & Galvin, A. B. 1995, *SSRv*, **72**, 71
 von Steiger, R., & Zurbuchen, T. H. 2006, *GeoRL*, **33**, L09103
 Winske, D. 1985, *SSRv*, **42**, 53
 Winske, D., & Omid, N. 1993, in *Computer Space Physics: Simulation Techniques and Software*, ed. H. Matsumoto & Y. Omura (Tokyo: Terra Scientific), 103
 Wong, H. K., & Goldstein, M. L. 1986, *JGR*, **91**, 5617